Full title :

Understanding evolutionary and functional relationships of RNA polymerases in plant and fungal viruses through structural modeling and divergence date estimations

Short title : Understanding RNA polymerase evolution in plant and fungal viruses

Authors :

Jérôme Gracy[1], Mahan Ghafari[2], Gilles Labesse[1], Denis Fargette[3], Eugénie Hébrard[3*]

[1]Centre de Biochimie Structurale, Montpellier, France

[2]Department of Biology, University of Oxford, UK

[3]PHIM Plant Health Institute, Univ Montpellier, IRD, CIRAD, INRAE, Institut Agro, Montpellier, France

*correspondence : eugenie.hebrard@ird.fr

Abstract

RNA-dependent RNA polymerases (RdRps) are crucial for replication of RNA viruses and serve as key marker genes for defining deep taxonomic ranks and for understanding viral evolutionary history. Despite shared functions and conserved amino acid motifs, the high genetic diversity of RdRps complicates precise sequence comparisons across viral families, hindering accurate taxonomic classification of new species – especially important at the age of metagenomics. When available, three-dimensional (3D) RdRp structures can help address these challenges through structure-based alignments. However, such structures are scarce for understudied viruses infecting fungi and plants, preventing the investigation of their ecological and evolutionary links.

In this study, we focused on the highy divergent order *Sobelivirales*. Using deep-learning structural modeling, we generated highly reliable 3D models on 20 representative viral species. Multiple structural alignment enabled the reconstruction of a robust phylogeny with improved quality and length. Based on this phylogeny, we proposed revisions of existing viral families and reclassified genera. Clade divergence dates were then estimated using the Prisoner of War model, which has previously revealed the ancient origin of the genus *Sobemovirus*. We provided here the first divergence time estimation between these plant and fungal viruses, dating back to 26.6 million years before present - significantly more recent than the divergence between their respective hosts. Our amino acid conservation analysis, validated on 99 other viral species, also identified molecular signatures of sobeliviral families and genera, which could help in future taxonomic assignment and diagnostic tools development. This interdisciplinary approach integrating structure modeling and date estimations offers new insights into the evolutionary divergence between fungus and plant viruses, with potential applications to other viral orders and families.

Author summary

RNA-dependent RNA polymerases (RdRps) are essential for RNA virus replication and serve as important markers for classifying viruses and understanding their evolution. However, with the rising popularity of metagenomics and discovery of viruses with high genetic diversity in RdRps, it is difficult to compare viral families and accurately classify new species. When available, 3D structures of RdRps can help overcome this challenge through structural alignments.

In this study, we focused on the highly divergent order of the Sobelivirales, using deep-learning models to generate reliable 3D structures for 20 representative viral species. These structural alignments allowed us to build a more accurate viral phylogeny. Based on this finding, we proposed updates to existing viral families and genera within the Sobelivirales order. We also estimated divergence dates using a model that previously uncovered the ancient origins of Sobemovirus. Notably, we provided the first estimate of when these plant and fungal viruses diverged - around 26.6 million years ago, which is much more recent than the separation of their hosts. We also identified molecular signatures that are useful for future virus classification and diagnosis, with potential applications to other viral groups.

58 **Introduction**

59 Recent advances in viral metagenomics have revealed how extensive and unexplored
60 viral diversity is, and have contributed significantly to a better understanding of viral evolution.
61 Major adaptations of viral taxonomic classification have been made to incorporate numerous
62 new lineages and their evolutionary links [1,2]. This includes the creation of novel upper ranks
63 and subdivisions such as classes and phyla [3]. The identification of viral hallmark genes
64 (VHG) facilitated the assignment of viral taxa into these novel groups [4,5]. Polymerases
65 especially RNA-dependent RNA polymerases (RdRp) represent one of the major groups of
66 VHG due to their crucial function for realm *Riboviria* (RNA viruses). RdRp comparative
67 analyses revealed unexpected relationships between some viral groups, prompting taxonomic
68 reassessments and modifications. For example, the establishment of the order *Reovirales* and
69 the dissolution of the family *Reoviridae* by the International Committee on Taxonomy of
70 Viruses (ICTV) were informed by detailed RdRp analyses [6]. This new ordering approach
71 which groups viruses with a shared replication strategy and a conserved RdRp core has allowed
72 *Reovirales* to be further subdivised into the families *Sedoreovirinae* and *Spinareovirinae*, based
73 on both major differences on the arrangement of RdRp conserved motifs and on the coat protein
74 (CP) morphology - the other crucial VHG. Similarly, the family *Luteoviridae* had initially
75 grouped the genera *Luteovirus* and *Polerovirus*, primarly due to their similar circulative
76 transmission mode mediated by aphids and the related readthrough domain of their CP.
77 However, based on the low sequence similarity of their RdRps, the family *Luteoviridae* was
78 abolished and the two genera were subsequently reassigned to the families *Tombusviridae* or
79 *Solemoviridae*, respectively [7].

80 Viral RdRps are monomeric proteins responsible for synthesizing complementary RNA
81 strands from a template RNA. They exhibit an overall structure often likened to a cupped human

82 right hand in which the fingers and thumb domains interact to form a characteristic central
83 tunnel (for review [8–11]). The palm domain is formed by a β-sheet with three to six β-strands
84 above two helices, the fingers domain is a mixed α/β structure and the thumb domain is highly
85 variable with a predominantly helical structure. The fingers and thumb domains contribute to
86 the RdRp overall stability and proper positioning of the RNA template and nascent RNA strand.
87 The palm domain is essential for the accurate and efficient RNA chain elongation. It allows the
88 positioning of the primer 3'OH, or the viral protein genome-linked (VPg) depending on the viral
89 taxon, the binding of incoming nucleotides and their incorporation to the RNA chain using two
90 metal ions as cofactors. Comparisons of RdRp sequences of diverse viral groups has identified
91 short linear motifs of highly conserved amino acids [12,13]. Five motifs (A-E) were reported
92 in the palm domain, two motifs (F and G) in the fingers domain and one putative and less
93 conserved motif (H) in the thumb domain. High throughput taxonomic assignment were often
94 based on ABC motifs [14–16]. Analyzing the three-dimensional (3D) structures of RdRps later
95 identified larger protein segments referred to as homomorphs, determined by structural
96 similarities rather than sequence composition [17]. However, for certain viral phyla like those
97 of plant and fungus viruses, lacking 3D structures, pose challenges to compare RdRps and to
98 reveal their phylogenetic relationships. To address this challenge, multiple protein alignments
99 were restricted to the central RdRp palm domain, using classical algorithms combined with
100 manual refinements based on available 3D structures from taxonomically less related viruses,
101 such as animal or human viruses. This approach led to the creation of the kingdom
102 *Orthornavirae* [4].

103 Although the monophyly of viruses in the order *Orthornavirae* has been established
104 based on comparison of their RdRps, reconstruction of their evolutionary history remains
105 difficult due to their strong, probably ancient, evolutionary divergence and the central role of
106 horizontal transfer of other viral genes in plant viruses [18]. In the picorna-like supergroup, now

107 referred as the phylum *Pisuviricota*, viral species share common structural and functional
108 features in RdRp. On the other hand, they also exhibit contrasting biological characteristics in
109 terms of host range (animals, insects, plants, fungi, protists), as well as variations in genomic
110 classification (positive single-stranded RNA or double-stranded RNA) and size (ranging from
111 the largest to the smallest RNA genomes) (see S1 Table). To investigate phylogeny of viral
112 taxons such as Pisiviricota can provide evolutionary hypotheses about the origins of these
113 distinct or shared traits. Viruses of fungi also named mycoviruses have been understudied, but
114 recent discoveries, such as cross-kingdom transmission events, highlight ecological and
115 evolutionary links with plant viruses [18–20]. In this study, we compared the RdRps inside the
116 order *Sobelivirales*, as markers of their common history to gain insights into host range
117 evolution. This order is one of the four orders of positive-sense single-stranded RNA (+ssRNA)
118 mycoviruses. It comprises families *Solemoviridae* and *Barnaviridae*, which contains plant and
119 fungus viruses, respectively. Solemoviridae includes four plant viral genera (*Sobemovirus*,
120 *Polerovirus*, *Enamovirus* and *Polemovirus*), while Barnaviridae consists of a single genus,
121 *Barnavirus*, composed of one approved and two tentative species infecting fungus (Table 1).
122 These families share the same genomic arrangement, chymotrypsine-like protease / VPg / RdRp
123 [21,22], but their sequence conservation is restricted to very short linear motifs. Similarities
124 between RdRp active sites of sobemovirus and polero-/enamovirus were noted as early as 1991
125 [12], leading finally to their taxonomic grouping in 2021 [23]. Close to poleroviruses, the
126 unique polemovirus species results from a recombination event with sobemovirus CP. Although
127 RdRp homologies between sobemoviruses and barnaviruses were proposed in 2008 [10], they
128 have not yet translated into any taxonomic revisions. Furthermore, a newly proposed genus of
129 fungal virus, *Hubsclerovirus*, has recently been assigned to the phytoviral family *Solemoviridae*
130 instead of *Barnaviridae* [24]. Thus, comparing more precisely the RdRps from these two viral
131 families would provide valuable insights into the complex history of plant and fungus viruses.

132 Our focus on Sobelivirales enabled the application of modern methodologies to
133 reconstruct their deep evolutionary histories. Notably, the genus *Sobemovirus* exemplifies a
134 unique case where the impact of time-dependent rate phenomenon (TDRP) on underestimation
135 divergence times using standard molecular clock methods has been considered using the
136 Prisoner of War model (PoW) [25,26]. Originally developped for reconstructing the
137 evolutionary history of human and animal viruses, the PoW model corrects for heterogeneous
138 and time-dependent evolutionary rates of viruses that may arise due to factors like epistasis,
139 nucleotide biases, and substitution saturation. The PoW model reproduces the empirically
140 observed power-law rate decay in estimated evolutionary rates of many RNA and DNA viruses
141 across deep evolutionary timescales. This method revealed a very ancient origin of sobemovirus
142 genus (over four million years) by contrast to the previous estimation based solely on the
143 extrapolation of short-term substitution rates [27]. The PoW model application needs three key
144 prerequisites - the detection of a temporal signal in time-stamped sequences, identification of
145 non-recombinant genomic regions, and a robust phylogenetic signal in the data. To overcome
146 the last issue at the high taxonomic rank of Sobelivirales, we leveraged both the structural
147 protein conservation and the advancements in deep-learning algorithms. Protein sequences
148 evolve at a faster rate than their corresponding structures. When proteins are distantly related,
149 which is the case in this group of virus sequences, mutational saturation becomes more likely
150 and interpretation of evolutionary signals becomes more challenging. The reliable structural
151 models predicted by Alphafold [28], which is using deep-learning for protein reconstruction,
152 allows us to build more accurate sequence alignments from highy divergent virus families [29]
153 collected from the vast number of metagenomics studies and to infer phylogenetic relationships
154 more accurately [16,30–32].

155 In this paper, applying AlphaFold on 20 representative species of sobelivirales revealed
156 the highly conserved folding of their RdRps. The subsequent superposition of all generated 3D

157 protein models with the multiple structure alignment algorithm mTM-align resulted in an robust
158 RdRp nucleotidic alignment reaching the quality requirements to estimate the divergence dates
159 with the PoW model at the scale of Sobelivirales. The analysis of amino acid conservation based
160 on the structural alignment also provided molecular signatures of sobeliviral families and
161 genera that will be useful to design taxonomical assignment and diagnostic tools in future. Our
162 interdisciplinary approach integrating structure modeling and date estimations on sobeliviral
163 RdRps provided new insights on the evolutionary divergence between fungal and plant viruses.

164 **Results**

165 Structural modeling

166 A set of 20 viral species was selected to be representative of Sobelivirales infecting
167 plants and fungi (Table 1). The RdRp structural models for these viruses were generated using
168 the Alphafold 2.2 algorithm. Additionally, three outgroup RdRps were identified, modeled and
169 incorporated into the initial dataset (Table 2). These homologues (MyCV, BeSV, XiNV),
170 present in the Uniprot database, were identified through metagenomics analyses from
171 arthropods or soil samples and found through AlphaFold based on their structural similarity
172 with sobeliviral RdRps. In total, more than 2,500 related proteins were aligned for each of the
173 23 target sequences. Predicted 3D models showed local distance difference test (plDDT) scores
174 ranging from 92% to 96%, indicating highly reliable structural models (Fig 1, see S2 Figure &
175 S3 File). We also conducted a preliminary analysis of *Heterocapsa circularisquama RNA virus*
176 (HcRNAV). This virus, which infects dinoflagellates, is currently the only described species of
177 the genus *Dinornavirus* in the family *Alvernaviridae* in the order *Sobelivirales*. While the
178 structural model of HcRNAV RdRp can be easily superimposed on that of RYMV RdRp, the
179 modeling scores were locally low along the protein, with 10 % of the residues having low-

180 confidence plDDT scores (< 60) (see S4 Figure). As a result, HcRNAV was excluded from
181 dowstream analyses.

182 The predicted 3D model of RYMV RdRp was initially compared to available 3D
183 structures of poliovirus (PV) and foot-and-mouth disease virus (FMDV), two well-studied
184 species of picornavirales in the phylum *Pisuviricota* [33]. The characteristic fingers-palm-
185 thumb organization was observed in all three structures (Fig 2, see S5 Figure & S6 File).
186 Although conservation between RYMV and PV/FMDV sequences was low (~10% identity)
187 except in the RdRp motifs, the nature and 3D orientation of most secondary structural elements
188 (α-helices and β-sheets) were preserved across all three structures. The central part of the
189 protein, which forms the conserved palm domain, showed high local structural similarity, with
190 root mean square deviations (RMSD) below 1 angstrom (Å). However, in this domain, there
191 was a larger number of β-strand elements which are longer in RYMV compared to the two
192 picornaviruses. In contrast, the thumb domain, formed by α-helices at the C-terminal part of
193 RdRps, was smaller in the predicted RYMV structure. At the N-terminal region, a conserved
194 feature of picornavirales RdRps was observed: the index finger interacted with the top of the
195 thumb, trapping the ring finger beneath it. Additionally, the orientation of the « pinky finger
196 helix », which has been previously described to distinguish two picornavirales groups including
197 FMDV or PV [33], would bring the predicted structure of RYMV closer to that of FMDV.

198 Structural alignment

199 Each RdRp 3D model of the 23 sobelivirales was structurally aligned using the mTM-
200 align algorithm [34]. We firstly analyzed the superimpositions of the models inside the same
201 genus (Fig 3). Given the sequence similarity between the RdRps of polemovirus and
202 poleroviruses (~75%), they were grouped together as « poler/moviruses » for the remainder of
203 the analyses. Intra-genus model superpositions revealed a high degree of structural similarity
204 in the alpha-carbon traces, with maximum RMSD below 1.3 Å. The least divergent structures

205 were found among poler/moviruses (0.68 Å) while hubscleroviruses and enamoviruses showed
206 intermediate values (1.10 Å and 1.12 Å, respectively). Higher RMSD values were observed for
207 sobemoviruses and barnaviruses (1.26 Å and 1.29 Å), primarly due to two main structural
208 variations: the distinct loop lengths at the thumb joint in sobemoviruses and at the edge of the
209 palm in barnaviruses, referred to here as the « orange loop » and the « light blue loop ».
210 However, we noted that unlike the « orange loop », the « light blue loop » exhibited lower
211 plDDT values (<70), indicating that the 3D conformation of this loop was uncertain. The three
212 outgroups exhibited greater structural divergence, with a maximum RMSD of 1.84 Å, which
213 was consistently localized to the external domains of the RdRp.

214 The 3D overlay of the 23 RdRps confirmed the global conservation of the structure of
215 sobeliviral RdRps (1.9 Å < RMSD < 2.5 Å) (Fig 4). While the RdRp core was highly conserved,
216 the main structural differences were observed on the protein surface, particularly in external
217 loops. In addition to the variable loops previously identified at the intra-genus level, the global
218 model superimposition revealed secondary structure elements specific to certain genera. For
219 instance, a longer loop was found in the wrist domain of barnavirus RdRps, which we refer to
220 as the « yellow loop ». Again, low plDDT values were observed in this barnaviral loop. In
221 poler/movirus and enamovirus RdRps, a supplementary helix and a longer loop, named here
222 the « green helix » and « red loop », were identified at the thumb junction and the thumb tip,
223 respectively (Fig 4). These specific secondary elements showed high plDDT scores (>90-80).
224 Additionally, the « light blue loop », found to be variable among barnaviruses but with
225 relatively low plDDT values, was also longer in hubscleroviruses compared to other sobeliviral
226 genera but with high plDDT scores (>90). Notably, the amino-terminal extremity of all
227 sobeliviral RdRps studied forms a β-strand, interacting with other strands of the middle and
228 ring fingers (Fig 4). At this inter-genera taxonomic level, it is the first time that an extra domain
229 has been explicitly included in the sequence alignment.

230 The amino acid alignment of the 23 RdRps from plant and fungal viruses has a mean
231 length of 459 residues across 649 sites (Fig 5). Amino acid conservation was notably low, with
232 only 31 out of 459 residues being strictly conserved (less than 7% of the mean length). Half of
233 these conserved residues are located within well-characterized RdRp motifs, including a third
234 within the ABC motifs. As expected, the solvent accessibility scores and predicted secondary
235 structure elements were well conserved along the linear sequences (see S7 File). The 3D
236 modeling facilitated alignment and optimization of gap positions and lengths. We observed
237 sequence clustering based on their secondary structure elements, which reflected both intra-
238 and inter-genus relationships. For example, positions 56-59 formed an α-helix in both
239 poler/movirus and enamovirus RdRps, while positions 118-130 folded as coil + 3_{10} helix in
240 both hubsclerovirus and sobemovirus polymerases.

241 The insertion/deletion (indels) of gaps to account for longer secondary structure
242 elements is heterogeneously distributed depending on the domains and viral species. These
243 indels corresponded to domains identified through the global superimposition of the 3D models
244 (Fig 4 & 5). Some indels were specific to individual genera, such as those for the « yellow
245 loop » at positions 492-507 in barnaviruses and the « orange loop » at positions 557-565 in
246 sobemoviruses. Other indels were shared between two genera, such as those for the « green
247 helix » and « red loop » at positions 370-380 and 604-609 in both poler/mo- and enamoviruses,
248 and those for the « light blue loop » at positions 138-186 found in barnaviruses and
249 husclerovirus.

250 Phylogeny and divergence date estimation

251 The structural alignment was translated into a multiple sequence alignment of nucleic
252 acids by replacing each amino acid by its corresponding codon (see S8 File), which was used
253 to construct the maximum-likelihood phylogenetic tree of Sobelivirales using the GTR+G+I

254 substitution model in PhyML (Fig 6). The outgroups formed a well-supported cluster and
255 contributed to reveal two main clades (with high bootstrap supports), referred to as Polena- and
256 Sobarna- throughout the text. Within the Polena-clade, the phylogenetic relationships between
257 poler/moviruses and enamoviruses were confirmed. In the Sobarna-clade, phylogenetic links
258 between plant sobemoviruses and fungal barna-/hubsclerovirus were highlighted, with a
259 bootsptrap value of 90, establishing this monophyletic group for the first time. However, the
260 phylogenetic relationships between hubscleroviruses and sobemoviruses lacked strong support.

261 The time-scaled phylogenetic history for the 20 Sobelivirales was constructed using the
262 PoW model applied to the structural alignment. According to this analysis, the most recent
263 common ancestor (TMRCA) of sobemoviruses dates back to 2.3 million years before present
264 (BP) (95% highest posterior density (HPD): 1.3-3.5 million years BP) (Fig 7), aligning closely
265 with a recent estimate [26]. The divergence time of the Polenamo-clade was estimated to 5.3
266 (95% HPD: 3.4–7.9) million years BP. The findings here provides the first estimate of the
267 TMRCA for fungal (barna)viruses, which dates back to 3 (95% HPD: 1.8-5.0) million years
268 BP, and for the Sobarna-clade to 17.7 (95% HPD: 12.2– 24.8) million years BP. Furthermore,
269 the analysis here offers the first estimation of the TMRCA of the Sobelivirales order, reaching
270 back to 26.6 (95% HPD: 19.2-34.8) million years BP, which is nearly ten times older than the
271 origins of sobemoviruses.

272 Polymerase evolution

273 The RdRp core and active sites within the central tunnel of Sobelivirales were found to
274 be highly conserved across all genera, despite significant divergence in their protein sequences
275 (see S9 Figure). In contrast, genus-specific residues were evenly distributed around the core
276 without being spatially clustered (data not shown). In order to take phylogenic data into account
277 in the study of the evolution of structure/function relationships of sobeliviral polymerases, we

278 analyzed sequence conservation by comparing the Polena- versus Sobarna- clades after
279 exclusion of the three outgroups (see S10 File & S11 Table). We identified 35 clade-specific
280 residues - i.e. amino acids strictly present (or physico-chemically similar) in all sequences of
281 one clade and strictly absent from sequences of the other clade. These residues were located on
282 31 polymorphic sites in the RdRps. Of these, 25 residues were strictly conserved : 4/11 in the
283 sobarnaviral sequences and 21/24 in the polenaviral sequences (see S11 Table). Six clade-
284 specific residues were found within the conserved RdRp motifs – three in the palm domain and
285 three in the fingers domains.

286 To validate these clade-specific residues, 99 additional sobeliviral sequences were
287 incorporated into our aligned dataset, resulting in a total dataset of 119 sequences, which
288 included all ICTV-recognized viral species in the studied genera (see S12 Table & S13 File).
289 Almost 70% (24/35) of the clade-specific polymorphisms were confirmed, including 3/4 and
290 10/21 strictly conserved residues for the Sobarna- and Polena-clades, respectively (Table 3).
291 Two new Sobarna-specific residues were detected in conserved motifs of the extended dataset :
292 a serine and a histidine within Motifs G and D, respectively, at positions 188 and 486 (referring
293 to the alignment with 20 sequences). In the Sobarna-clade, residues at positions 486 and 489
294 were particularly notable for their 3D positions within Motif D - residue 489K/R pointed into
295 the central tunnel, while 486H/K was likely stabilized by residue 365E (Fig 8). In the Polena-
296 clade, a strictly conserved lysine at position 263 within Motif F also pointed into the central
297 tunnel, alongside the conserved sobeliviral lysine at position 266 (Fig 8). This analysis revealed
298 molecular signatures of these deeply divergent clades, refining the definitions of the conserved
299 motifs (Fig 9). In addition to clade-specific polymorphic positions such as 354I/C, 468S/A and
300 188S/G, certain residues were strictly conserved across sobelivirales, including 355-356SG,
301 261-262PH, 512-514FCS in Motifs A, F and E, respectively. The specificity of these conserved
302 residues to the sobeliviral order have to be tested by analyzing a larger dataset of RdRp

sequences from species of other viral orders. Moreover, genera-specific features idenfied on the structural alignment of 20 sequences were confirmed on the expanded corpus. Notably, the polena- « green helix » upstream Motif A and the polena- « red loop » dowstream Motif H provided robust indel signatures. The sobemoviral « orange loop » between Motifs D and E was also validated, appearing less variable than previously observed in the smaller corpus of 20 sequences.

311 **Discussion**

312 Protein structure modeling has proved effective in addressing some of the challenges to
313 making reliable sequence alignments posed by low sequence conservation at high taxonomic
314 levels. In this study, we used AlphaFold models to produce a robust and extensive sequence
315 alignement of sobeliviral RdRps, for the first time at this taxonomic level. Although initially
316 based on a limited set of sequences, the alignment was extensively validated using a full set of
317 known viral species in this order. Minor discrepancies, however, were observed in gap positions
318 at carboxy-terminal extremity of RdRp. In addition, the limited number of known
319 hubscleroviruses and barnaviruses prevented the validation of some features such as the « light
320 blue loop » and « yellow loop », respectively. Protein structure modeling successfully provided
321 high confidence supports that complemented classical functional motifs, serving as anchor
322 points. Notably, the RdRp extremities which are typically trimmed upstream of motif G and
323 downstream of motif E - deleting approximatively 150 residues - were very well predicted by
324 Alphafold, with plDDT exceeding 90%, and showing high structural similarity (RMSD < 2 Å).
325 Here, we considered the amino-terminal extremity of RdRp and its intra-molecular interactions,
326 improving the alignement length and quality.

327 In addition to generating robust structure models, Alphafold helps to identify new
328 homologues in databases. In this study, we selected three outgroups from metagenomic data
329 based on their genetic distance from the 20 initial sequences. Generally closer than
330 alvernaviruses, these outgroups served as a reliable reference for rooting the phylogenetic tree
331 and enhancing the quality of the phylogenetic analysis. We evaluated the accuracy of our
332 structural alignement to traditional alignment algorithms. The residue pairing between our
333 structural alignment and MAFFT, Clustal Omega, and MUSCLE showed differences of 21%,
334 23%, and 30%, respectively. Most of these differences were observed in the loop/coil regions

335 as well as in the amino- and carboxy-terminal extremities of the protein (see S14 File).
336 However, these differences had minimal impact on tree topology as they mainly concerned the
337 outgroup alignment (see S15 Figure). MUSCLE produced results similar to mTM-align, while
338 Clustal Omega and MAFFT failed to detect phylogenetic relationships between
339 hubscleroviruses and sobemovirus. Furthermore, Clustal Omega yielded low internal node
340 support at the sobemovirus / barnavirus split. The lower accuracy of Clustal Omega compared
341 to MUSCLE and MAFFT has been already reported for structural alignments of Flaviviridae
342 glycoproteins [31].

343 The phylogenic analysis led to a new taxonomic proposal : the creation of two new
344 tentative families Polenaviridae and Sobarnaviridae, replacing Solemoviridae and
345 Barnaviridae. By assessing the conservation of the structural alignment, we enriched the
346 common conserved motifs, identified molecular signatures of the new tentative families, and
347 revealed structural diversity (e.g., loop lengths) that can be used as marker of viral genera.
348 Interestingly, newly identified putative sobemo-like and sobeli-like viruses often represent a
349 significant portion of newly discovered plant and fungus taxa within environnemental viromes
350 [16,35–38]. Extending this approach in the near future will accelerate their taxonomic
351 classification, a priority for virus research [39]. Additionally, these RdRp features could be
352 useful for the development of molecular tools for diagnostic and detection.

353 The efficiency of our integrative approach was demonstrated at the taxonomic rank of
354 order/family and could be implemented to other clades, such as fungal viruses in the phylum
355 *Pisuviricota*, such as *Polymycoviridae* and *Yadokarivirales*, currently unassigned at the family
356 and order levels, respectively. However, this approach requires some level of structural
357 similarity below which comparisons are not recommended. To assess this limit, we predicted
358 3D models of the RdRp of *Luteovirus pavhordei* (previously named BYDV-pav) and

359 *Dianthovirus trifolii* (previously named RCNMV), since the former was previously classified
360 in the family *Luteoviridae* with the poleroviruses and is now classified with the latter in
361 *Tombusviridae* (Order *Totivirales*, Class *Tolucaviricetes*, phylum *Kitrinoviricota*) [7]. These
362 3D models were aligned with one representative of each six genera using the same method as
363 described above (see S16 File). Although the core of all three RdRps showed good sequence
364 and structure similarity, the overlay score on the full-length protein was low (3.3 Å > RMSD >
365 3.5Å). As expected, most of the Sobarna-and Polena-specific residues in the motifs, were not
366 shared with the two totivirales analyzed. The unique exception was observed in the motif G for
367 which *Luteovirus pavhordei* showed the same pattern as sobarnavirid sequences (188-189SP).
368 Noteworthy, half of the sobeliviral-conserved residues in Motifs A, F and E were also present
369 in the two totivirales analyzed (355S, 262H, 512-513FC, respectively) suggesting that these
370 residues were not strictly specific. These preliminary analyses should be continued and
371 expanded in the future. By contrast to the core, the external loops of the two totiviral RdRps
372 analyzed here showed very low structural similarity with the sobeliviral ones. In addition,
373 neither the « green helix » and « red loop » nor the « orange loop », the secondary structure
374 elements specific to polenavirids and sobarnavirids, respectively, were observed. Consequently,
375 we considered that entire RdRps of luteoviruses were significantly too distant to RdRps of
376 poleroviruses and sobelivirales to be aligned accurately with our structural approach.

377 Furthermore, structural similarity does not always imply phylogenic relationships. As
378 mentionned earlier, for the picorna-like supergroup, the hypothesis of convergent evolution
379 cannot be excluded [5]. Picornaviruses show both structural and functional similarities with
380 sobelivirales, such as the use of a Viral Protein genome-linked (VPg) to prime RNA replication
381 by the RdRp. However, picornaviral VPg are very small (~20 residues) and are cleaved from
382 the RdRp by a viral protease located downtream of the VPg domain. In contrast, the
383 sobarnavirids and polenavirids share a conserved genomic organization

384 (protease/VPg/polymerase) and have larger VPgs (80-150 residues), which likely result in or
385 induce specific molecular mechanisms. While interactions between VPg and RdRps and their
386 structure-function relationships have been extensively studied in human and animal viruses,
387 very little data exist for plant viruses. Our approach could help to fill this knowledge gap, or at
388 least provide a better understanding of plant RdRp features through *in silico* comparative
389 analyses.

390 For example, the comparative analysis of Motif E, unique to RdRps compared to other
391 polymerases, offers a good starting point for better understanding of some of the plant RdRp
392 features. The amino acid composition of this motif is directly linked to the viral replication
393 strategy, using protein priming (VPg) or not. Described as « primer grip », this motif has been
394 shown to help correctly position the 3' OH end of the primer strand [9,17]. In picornaviral
395 RdRps, the conserved phenylalanine in Motif E, which faces Motif C, is followed by two
396 residues with relatively long side chains (phenylalanine-leucine-lysine, FLK), while in
397 flaviviral RdRps, the central channel is narrower, and these residues have rather short side
398 chains (phenylalanine-cysteine-serine, FCS). Interestingly, plant and fungus sobeliviral RdRps
399 share the same conserved Motif E as flavivirids. Additionaly, the homomorph that contains
400 Motif E forms part of the NTP entry tunnel and can vary in lenght depending on the viral
401 species. Sobemoviruses exhibit a longer « orange loop » at the thumb joint compared to other
402 members of sobelivirales, another unexpected similarity with flaviviral hepatitis virus C.

403 At a different taxonomic scale, Motif D illustrates the common evolutionary history of
404 plant and fungus sobeliviral RdRps. This motif influences the rate of nucleotide addition to the
405 nascent RNA strand. Characterized by a glycine hinge and a positively charged lysine, both
406 located in similar positions across available RdRp crystal structures, the distance inside the
407 linear sequence between these two conserved residues varies across different viral families [9].

408 In the Sobarnaviridae clade, lysine (or its equivalent arginine) is conserved at position N+4, i.e.
409 position 489 (in the reference alignement of 20 sequences) (Fig 9). In the Polenaviridae clade,
410 our initial analysis was too stringent to detect the conserved lysine, as one species out of 89 had
411 a non-conserved hydrophobic isoleucine at this position. However, when *Enamovirus CLEV*
412 was excluded from the dataset, the conserved lysine was found at position N+2 – i.e. position
413 487, with its orientation differing from the sobernaviridae lysine in the 3D structural model.
414 Motif D has been shown to influence not only incorporation speed but also fidelity, both of
415 which are closely linked to viral pathogenesis and virulence. For example, increased fidelity in
416 a poliovirus mutant has been associated with viral attenuation [40].

417 The structural differences and evolutionary distances between RdRps of sobemoviruses
418 and poleroviruses (two phytovirus genera in the order *Sobelivirales*) were found to be greater
419 than those between sobemoviruses and barnaviruses (a mycovirus genus in the family
420 *Barnaviridae*) as well as hubscleroviruses (a mycovirus genus in the family *Solemoviridae*).
421 Given the role of RdRp as a major marker of viral evolutionary history, our results confirmed
422 that horizontal viral transfert(s) (HVT) between plant/fungal viruses occured in the Order
423 *Sobelivirales*. The direction of the HVT(s) cannot yet be determined without further data on the
424 hosts of metagenomic sequences we used as outgroups. Using an interdisciplinary approach,
425 we provided the first divergence time estimation between these plant and fungal viruses, dating
426 back to ~26 million years BP. The TDRP-corrected evolutionary history of sobelivirales was
427 extended five thousand times far beyond previous estimates [27]. However, we note that this
428 estimate may reflect a conservative timeframe based on current methodologies, as our
429 understanding of TDRP and application of the PoW model has primarily been at the genus and
430 family levels. With future advances in modeling and expanded data, these divergence times
431 could potentially be revised further back. Yet, even with our current conservative estimates, the
432 divergence time remains more recent than the divergence between the respective plant and

433 fungal hosts (>400 millions years) [41], suggesting that a strict virus-host co-evolution
434 hypothesis not fully explain these evolutionary relationships. Other lineages of mycoviruses
435 either with single- or double-stranded RNA genomes showed close phylogenetic relationships
436 with plant viruses at different taxonomical ranks [18,20,42], suggesting that taxonomy of these
437 viruses should rather be viewed as a continuum. An interdisciplinary approach at the interface
438 of biophysics, bioinformatics, and virology should be encouraged to better understand
439 evolution, interactions and biological mechanisms of myco- and phytoviruses.
440

441 **Material and methods**

442 Sequence selection

443 The sobeliviral dataset initially consisted of 20 species from six genera (Table 1). Six
444 sobemoviruses including four recently described (ArtVA, CyCMV, PLYV, XYDV), four
445 poleroviruses, four enamoviruses, one polemovirus, two hubscleroviruses including one
446 candidate species, and three barnaviruses including two candidate species. Complementary
447 analyses were performed on *Heterocapsa circularisquama RNA virus* (HcRNAV, accession
448 NC007518, *Dinornavirus, Alvernaviridae, Sobelivirales*), on *Luteovirus pavhordei* (BYDV-
449 pav, accession OM046620, *Luteovirus, Tombusviridae, Tolivirales*) and on *Dianthovirus trifolii*
450 (RCNMV, accession OL311680, *Dianthovirus, Tombusviridae, Tolivirales*).

451 The validation dataset consisted of 99 sequences of sobelivirales species made of all the
452 ICTV viral species available in the studied genera. In addition to the two hubscleroviruses, the
453 three barnaviruses and the polemovirus already cited, the complete corpus consisted of 25
454 sobemoviruses, 73 poleroviruses and 15 enamoviruses (see S12 Table).

455 3D model prediction

456 The structures of the corresponding RdRps were predicted using a locally installed
457 version of Alphafold 2.2 [28]. For each sequence, 5 models were generated and relaxed using
458 default Alphafold parameters. All homologues detected by Jackhmmer [43] in the Uniprot
459 database (https://www.uniprot.org/) during these 20 Alphafold runs were then clustered using
460 kClust into groups of proteins sharing at least both 80% sequence identity and 50% sequence
461 overlap [44]. The representative sequences of each group were then aligned using MAFFT [45]
462 and a phylogenetic tree was derived from the alignment using FastME [46]. From this tree,
463 three new proteins were selected forming an outlier group (MyCV, BeSV, XiNV) (Table 2).

464 The 3D structure of these new proteins, as well as RdRps of HcRNAV, BYDV-pav and
465 RCNMV, were also predicted using Alphafold.

466 Evaluation of 3D models

467 One representative of each 6 viral genera was selected - RYMV (*Sobemovirus*), PLRV
468 (*Polerovirus*), PeMV (*Enamovirus*), MBV (*Barnavirus*), HuSRV (*Hubsclerovirus*), XyNV
469 (outgroups). The best RdRp 3D models predicted by Alphafold for these viral species were
470 structurally aligned using mTM-align [34]. The pLDDT reliability scores available in the B-
471 factor field of each Alphafold model were coded as integers (0=0-10, 1=10 -20, …, 9=90-100)
472 which were added to the mTM-align structural alignment with sequence identifiers suffixed by
473 .sc.PLDDT. This alignment is displayed in a web page where the aligned sequences and their
474 corresponding pLDDT scores are interfaced with 6 representative 3D models using Jsmol applet
475 and script [47]. Selected Alphafold models can displayed and customized by using the toggle
476 buttons and the popup menus from the right bottom panel and the colors of the amino acids or
477 pLDDT scores of one aligned sequence from the top panel can be projected on the selected 3D
478 structure(s) by clicking on the corresponding protein identifier in the top left panel (see S3 File).

479 The RYMV 3D model with highest Alphafold pLDDT scores was superposed to 1RA6
480 and 1U09 PDB structures of poliovirus (PV) and foot-and-mouth disease virus (FMDV) RdRps,
481 respectively, using mTM-align. The sequence identity between the three proteins was
482 calculated after alignment with Ident and Sim software [48]. The observed Cα deviations, in
483 Angstroms, where added below the obtained structural alignment (identifier suffixed with
484 d3.RMSD_1ra6A an .d3.RMSD_1u09A). The Cα deviation colors can be projected onto one
485 of the displayed structures by cliking one of these identifiers (see S6 File).

486

487 Structural alignment construction

488 All the best 3D models predicted by Alphafold for the 23 virus proteins were structurally
489 aligned using mTM-align. The 23 analyzed proteins were clustered into 6 subgroups
490 (Sobemovirus, Barnavirus, Hubsclerovirus, Poler/movirus, Enamovirus and a subgroup of
491 outlier viruses). The best RdRp 3D model of the 23 sobelivirales were superimposed with the
492 other models inside its group using mTM-align. The RMSD between the aligned carbon alpha
493 atoms was calculated for each viral pair inside each subgroup, then the maximum and average
494 RMSD between subgroup pairs were computed.

495 We carefully delineated the polymerase domain shared by the 23 proteins by inspecting
496 both the positional conservation of the aligned sequences, the superposition of their predicted
497 secondary structures and the solvent accessibility (see S7 File). The secondary structure and the
498 solvent accessibility of each model residue was calculated using STRIDE [49] and the
499 positional conservation was calculated as the frequency of the most represented amino acid in
500 a given alignment column.

501 Phylogenetic analysis and time tree reconstruction with PoW model

502 The mTM-align structural alignment was translated into a multiple sequence alignment
503 of nucleic acids by replacing each amino acid by its corresponding codon (Table 1) (see S8
504 File). JModelTest 2 [50] was used to identify the best nucleotide substitution model for
505 phylogenetic analysis based on the Akaike Information Criterion. The Maximum-Likelihood
506 tree was then constructed with the General Time Reversible Model with an optimised rate
507 variation and class for invariant sites (GTR + G + I) using PhyML implemented in SeaView (v
508 5.05) [51]. The absence of recombination events between species was confirmed with the Phi
509 test [52]. The reliability of the phylogenetic tree nodes was estimated via a bootstrap resampling
510 procedure with 100 replicates. The phylogenetic tree was rooted using the outgroup branch.

511 We have also detected the homologous amino acid pairs which were identically aligned
512 between the mTM-align structural alignment and each multiple sequence alignment built using
513 respectively MAFFT [45], MUSCLE [53] and Clustal Omega [54]. The frequencies of shared
514 amino acid pairs were calculated both over the whole alignments and within each alignment
515 column (see S14 File).

516 We used the Prisoner of War (PoW) model of virus evolution to account for the power-
517 law decay in the substitution rate estimates of sobemoviruses, as described in Ghafari et al. [26],
518 where we also established the presence of a robust and representative molecular clock signal
519 for the RdRp locus for sobemoviruses. Briefly, the short-term substitution rate of RYMV's
520 polymerase gene, inferred from a standard molecular clock model was used as the baseline rate,
521 then ultrametric distance trees were constructed using the substitution rate at the fastest-
522 evolving rate group for our dataset with a strict molecular clock in BEAST (v 1.10.4) [55]. The
523 maximum clade credibility tree was constructed after 100 iterations using TreeAnnotator
524 v.1.10.4 and visualized through a lineages-through-time plot using the phytools library in R
525 [56].

526 Polymerase evolution

527 The analyzed proteins were clustered into 2 subgroups comparing the Polena- versus
528 Sobarna- clades. The three outgroups were not considered in this analysis (see S10 File). At
529 each site of this new mTM-align structural alignment, amino acids strictly present in all
530 sequences of one clade (or that were similar based on BLOSUM score ≥ 0) and strictly absent
531 from sequences of the other clade were considered as clade-specific residue. These conserved
532 residues specific to Sobarna- and Polena-clades were added to the mTm-align alignment as two
533 final consensus sequences suffixed by c1.PID and .c2.PID respectively. The location of these
534 signature residues can be highlighted on the displayed 3D model clicking one of the c1.PID and

.c2.PID identifier and by hovering the mouse pointer onto one of the consensus sequence. In the supplementary table, only strictly conserved or similar in all sequences of one clade were considered. Motif analysis was made with WebLogo v2.8.2 [57].

Acknowledgements

This work benefited from discussions with Aurore Comte and Nils Poulicard, other members of Virus/Cereal Interactions in Tropical Agroecosystems group and colleagues of Plant Health Institute Montpellier. This work was supported by the French Infrastructure for Integrated Structural Biology (FRISBI) ANR-10-INBS-0005.

Data and code availability

The code for the PoW model is available on GitHub https://github.com/mg878/PoW_model

All the data (including accession numbers) are provided within the main text and supporting information.

Competing interest

None.

Funding

None.

Author contribution

Writing (original draft) JG and EH; Writing -- review and editing all authors; Formal Analysis JG MG EH: Conceptualization all authors; Data Collection JG DF EH; Supervision EH. All authors reviewed and edited the manuscript.

Correspondence to Eugénie Hébrard (eugenie.hebrard@ird.fr).

559 **References**

560 1. Simmonds P, Adams MJ, Benkő M, Breitbart M, Brister JR, Carstens EB, et al. Virus taxonomy in
561 the age of metagenomics. Nat Rev Microbiol. 2017;15: 161–168. doi:10.1038/nrmicro.2016.177

562 2. Gorbalenya AE. Increasing the number of available ranks in virus taxonomy from five to ten and
563 adopting the Baltimore classes as taxa at the basal rank. Arch Virol. 2018;163: 2933–2936.
564 doi:10.1007/s00705-018-3915-6

565 3. Siddell SG, Walker PJ, Lefkowitz EJ, Mushegian AR, Adams MJ, Dutilh BE, et al. Additional
566 changes to taxonomy ratified in a special vote by the International Committee on Taxonomy of
567 Viruses (October 2018). Arch Virol. 2019;164: 943–946. doi:10.1007/s00705-018-04136-2

568 4. Koonin EV, Dolja VV, Krupovic M, Varsani A, Wolf YI, Yutin N, et al. Global Organization and
569 Proposed Megataxonomy of the Virus World. Microbiol Mol Biol Rev. 2020;84: e00061-19.
570 doi:10.1128/MMBR.00061-19

571 5. Wolf YI, Kazlauskas D, Iranzo J, Lucía-Sanz A, Kuhn JH, Krupovic M, et al. Origins and Evolution
572 of the Global RNA Virome. Racaniello VR, editor. mBio. 2018;9: e02329-18.
573 doi:10.1128/mBio.02329-18

574 6. Walker PJ, Siddell SG, Lefkowitz EJ, Mushegian AR, Adriaenssens EM, Alfenas-Zerbini P, et al.
575 Recent changes to virus taxonomy ratified by the International Committee on Taxonomy of
576 Viruses (2022). Arch Virol. 2022;167: 2429–2440. doi:10.1007/s00705-022-05516-5

577 7. Walker PJ, Siddell SG, Lefkowitz EJ, Mushegian AR, Adriaenssens EM, Alfenas-Zerbini P, et al.
578 Changes to virus taxonomy and to the International Code of Virus Classification and
579 Nomenclature ratified by the International Committee on Taxonomy of Viruses (2021). Arch
580 Virol. 2021;166: 2633–2648. doi:10.1007/s00705-021-05156-1

581 8. Ferrero D, Ferrer-Orta C, Verdaguer N. Viral RNA-Dependent RNA Polymerases: A Structural
582 Overview. In: Harris JR, Bhella D, editors. Virus Protein and Nucleoprotein Complexes.
583 Singapore: Springer Singapore; 2018. pp. 39–71. doi:10.1007/978-981-10-8456-0_3

584 9. Jácome R, Becerra A, Ponce de León S, Lazcano A. Structural Analysis of Monomeric RNA-
585 Dependent Polymerases: Evolutionary and Therapeutic Implications. Kuhn JH, editor. PLOS
586 ONE. 2015;10: e0139001. doi:10.1371/journal.pone.0139001

587 10. Koonin EV, Wolf YI, Nagasaki K, Dolja VV. The Big Bang of picorna-like virus evolution antedates
588 the radiation of eukaryotic supergroups. Nat Rev Microbiol. 2008;6: 925–939.
589 doi:10.1038/nrmicro2030

590 11. te Velthuis AJW. Common and unique features of viral RNA-dependent polymerases. Cell Mol
591 Life Sci. 2014;71: 4403–4420. doi:10.1007/s00018-014-1695-z

592 12. Koonin EV. The phylogeny of RNA-dependent RNA polymerases of positive-strand RNA viruses.
593 J Gen Virol. 1991;72: 2197–2206. doi:10.1099/0022-1317-72-9-2197

594 13. Poch O, Sauvaget I, Delarue M, Tordo N. Identification of four conserved motifs among the
595 RNA-dependent polymerase encoding elements. EMBO J. 1989;8: 3867–3874.
596 doi:10.1002/j.1460-2075.1989.tb08565.x

597 14. Charon J, Buchmann JP, Sadiq S, Holmes EC. RdRp-scan: A bioinformatic resource to identify
598 and annotate divergent RNA viruses in metagenomic sequence data. Virus Evol. 2022;8:
599 veac082. doi:10.1093/ve/veac082

600 15. Edgar RC, Taylor B, Lin V, Altman T, Barbera P, Meleshko D, et al. Petabase-scale sequence
601 alignment catalyses viral discovery. Nature. 2022;602: 142–147. doi:10.1038/s41586-021-
602 04332-2

603 16. Hou X, He Y, Fang P, Mei S-Q, Xu Z, Wu W-C, et al. Using artificial intelligence to document the
604 hidden RNA virosphere. Cell. 2024; S0092867424010857. doi:10.1016/j.cell.2024.09.027

605 17. Lang DM, Zemla AT, Zhou CLE. Highly similar structural frames link the template tunnel and NTP
606 entry tunnel to the exterior surface in RNA-dependent RNA polymerases. Nucleic Acids Res.
607 2013;41: 1464–1482. doi:10.1093/nar/gks1251

608 18. Dolja VV, Krupovic M, Koonin EV. Deep Roots and Splendid Boughs of the Global Plant Virome.
609 Annu Rev Phytopathol. 2020;58: 23–53. doi:10.1146/annurev-phyto-030320-041346

610 19. Andika IB, Tian M, Bian R, Cao X, Luo M, Kondo H, et al. Cross-Kingdom Interactions Between
611 Plant and Fungal Viruses. Annu Rev Virol. 2023;10: 119–138. doi:10.1146/annurev-virology-
612 111821-122539

613 20. Roossinck MJ. Evolutionary and ecological links between plant and fungal viruses. New Phytol.
614 2019;221: 86–92. doi:10.1111/nph.15364

615 21. Gorbalenya AE, Donchenko AP, Blinov VM, Koonin EV. Cysteine proteases of positive strand
616 RNA viruses and chymotrypsin-like serine proteases: A distinct protein superfamily with a
617 common structural fold. FEBS Lett. 1989;243: 103–114. doi:10.1016/0014-5793(89)80109-7

618 22. Revill PA, Davidson AD, Wright PJ. Mushroom Bacilliform Virus RNA: The Initiation of
619 Translation at the 5′ End of the Genome and Identification of the VPg. Virology. 1998;249: 231–
620 237. doi:10.1006/viro.1998.9345

621 23. Sõmera M, Fargette D, Hébrard E, Sarmiento C, ICTV Report Consortium. ICTV Virus Taxonomy
622 Profile: Solemoviridae 2021: This article is part of the ICTV Virus Taxonomy Profiles collection. J
623 Gen Virol. 2021;102. doi:10.1099/jgv.0.001707

624 24. Simmonds P, Adriaenssens EM, Lefkowitz EJ, Oksanen HM, Siddell SG, Zerbini FM, et al.
625 Changes to virus taxonomy and the ICTV Statutes ratified by the International Committee on
626 Taxonomy of Viruses (2024). Arch Virol. 2024;169: 236. doi:10.1007/s00705-024-06143-y

627 25. Ghafari M, Simmonds P, Pybus OG, Katzourakis A. A mechanistic evolutionary model explains
628 the time-dependent pattern of substitution rates in viruses. Curr Biol. 2021;31: 4689-4696.e5.
629 doi:10.1016/j.cub.2021.08.020

630 26. Ghafari M, Sõmera M, Sarmiento C, Niehl A, Hébrard E, Tsoleridis T, et al. Revisiting the origins
631 of the Sobemovirus genus: A case for ancient origins of plant viruses. Nagy PD, editor. PLOS
632 Pathog. 2024;20: e1011911. doi:10.1371/journal.ppat.1011911

633 27. Fargette D, Pinel A, Rakotomalala M, Sangu E, Traoré O, Sérémé D, et al. *Rice Yellow Mottle*
634 *Virus* , an RNA Plant Virus, Evolves as Rapidly as Most RNA Animal Viruses. J Virol. 2008;82:
635 3584–3589. doi:10.1128/JVI.02506-07

636 28. Jumper J, Evans R, Pritzel A, Green T, Figurnov M, Ronneberger O, et al. Highly accurate protein
637 structure prediction with AlphaFold. Nature. 2021;596: 583–589. doi:10.1038/s41586-021-
638 03819-2

639 29. Carpentier M, Chomilier J. Protein multiple alignments: sequence-based versus structure-based
640 programs. Valencia A, editor. Bioinformatics. 2019;35: 3970–3980.
641 doi:10.1093/bioinformatics/btz236

642 30. Gutnik D, Evseev P, Miroshnikov K, Shneider M. Using AlphaFold Predictions in Viral Research.
643 Curr Issues Mol Biol. 2023;45: 3705–3732. doi:10.3390/cimb45040240

644 31. Mifsud JCO, Lytras S, Oliver MR, Toon K, Costa VA, Holmes EC, et al. Mapping glycoprotein
645 structure reveals Flaviviridae evolutionary history. Nature. 2024;633: 695–703.
646 doi:10.1038/s41586-024-07899-8

647 32. Nino Barreat JG, Katzourakis A. Deep mining reveals the diversity of endogenous viral elements
648 in vertebrate genomes. Nat Microbiol. 2024;9: 3013–3024. doi:10.1038/s41564-024-01825-4

649 33. Peersen OB. Picornaviral polymerase structure, function, and fidelity modulation. Virus Res.
650 2017;234: 4–20. doi:10.1016/j.virusres.2017.01.026

651 34. Dong R, Peng Z, Zhang Y, Yang J. mTM-align: an algorithm for fast and accurate multiple protein
652 structure alignment. Valencia A, editor. Bioinformatics. 2018;34: 1719–1725.
653 doi:10.1093/bioinformatics/btx828

654 35. Chen Y-M, Sadiq S, Tian J-H, Chen X, Lin X-D, Shen J-J, et al. RNA viromes from terrestrial sites
655 across China expand environmental viral diversity. Nat Microbiol. 2022;7: 1312–1323.
656 doi:10.1038/s41564-022-01180-2

657 36. Duarte MF, De Andrade IA, Silva JMF, De Melo FL, Machado AM, Inoue-Nagata AK, et al.
658 Metagenomic analyses of plant virus sequences in sewage water for plant viruses monitoring.
659 Trop Plant Pathol. 2023;48: 408–416. doi:10.1007/s40858-023-00575-8

660 37. Maksimović O, Bačnik K, Rivarez MPS, Vučurović A, Mehle N, Ravnikar M, et al. Virome analysis
661 of irrigation water sources provides extensive insights into the diversity and distribution of
662 plant viruses in agroecosystems. Water Res. 2024;249: 120712.
663 doi:10.1016/j.watres.2023.120712

664 38. Shi M, Lin X-D, Tian J-H, Chen L-J, Chen X, Li C-X, et al. Redefining the invertebrate RNA
665 virosphere. Nature. 2016;540: 539–543. doi:10.1038/nature20167

666 39. Gorbalenya AE, Siddell SG. Recognizing species as a new focus of virus research. Morrison TE,
667 editor. PLOS Pathog. 2021;17: e1009318. doi:10.1371/journal.ppat.1009318

668 40. Castro C, Smidansky ED, Arnold JJ, Maksimchuk KR, Moustafa I, Uchida A, et al. Nucleic acid
669 polymerases use a general acid for nucleotidyl transfer. Nat Struct Mol Biol. 2009;16: 212–218.
670 doi:10.1038/nsmb.1540

671 41. Selosse, Marc-André, Strullu-Derrien, Christine, Martin, Francis M., Kamoun, Sophien, Kenrick,
672 Paul. Plants, fungi and oomycetes: a 400-million year affair that shapes the biosphere. New
673 Phytol. 2015;206: 501–506. Available: https://www.jstor.org/stable/newphytologist.206.2.501

674 42. Ghabrial SA, Castón JR, Jiang D, Nibert ML, Suzuki N. 50-plus years of fungal viruses. Virology.
675 2015;479–480: 356–368. doi:10.1016/j.virol.2015.02.034

676 43. Johnson LS, Eddy SR, Portugaly E. Hidden Markov model speed heuristic and iterative HMM
677 search procedure. BMC Bioinformatics. 2010;11: 431. doi:10.1186/1471-2105-11-431

678 44. Hauser M, Mayer CE, Söding J. kClust: fast and sensitive clustering of large protein sequence
679 databases. BMC Bioinformatics. 2013;14: 248. doi:10.1186/1471-2105-14-248

680 45. Katoh K, Standley DM. MAFFT Multiple Sequence Alignment Software Version 7: Improvements
681 in Performance and Usability. Mol Biol Evol. 2013;30: 772–780. doi:10.1093/molbev/mst010

682 46. Lefort V, Desper R, Gascuel O. FastME 2.0: A Comprehensive, Accurate, and Fast Distance-
683 Based Phylogeny Inference Program: Table 1. Mol Biol Evol. 2015;32: 2798–2800.
684 doi:10.1093/molbev/msv150

685 47. Hanson RM. *Jmol* – a paradigm shift in crystallographic visualization. J Appl Crystallogr. 2010;43:
686 1250–1260. doi:10.1107/S0021889810030256

687 48. Stothard P. The Sequence Manipulation Suite: JavaScript Programs for Analyzing and
688 Formatting Protein and DNA Sequences. BioTechniques. 2000;28: 1102–1104.
689 doi:10.2144/00286ir01

690 49. Frishman D, Argos P. Knowledge-based protein secondary structure assignment. Proteins Struct
691 Funct Bioinforma. 1995;23: 566–579. doi:10.1002/prot.340230412

692 50. Darriba D, Taboada GL, Doallo R, Posada D. jModelTest 2: more models, new heuristics and
693 parallel computing. Nat Methods. 2012;9: 772–772. doi:10.1038/nmeth.2109

694 51. Guindon S, Gascuel O. A Simple, Fast, and Accurate Algorithm to Estimate Large Phylogenies by
695 Maximum Likelihood. Rannala B, editor. Syst Biol. 2003;52: 696–704.
696 doi:10.1080/10635150390235520

697 52. Bruen TC, Philippe H, Bryant D. A Simple and Robust Statistical Test for Detecting the Presence
698 of Recombination. Genetics. 2006;172: 2665–2681. doi:10.1534/genetics.105.048975

699 53. Edgar RC. MUSCLE: a multiple sequence alignment method with reduced time and space
700 complexity. BMC Bioinformatics. 2004;5: 113. doi:10.1186/1471-2105-5-113

701 54. Sievers F, Higgins DG. Clustal Omega for making accurate alignments of many protein
702 sequences. Protein Sci. 2018;27: 135–145. doi:10.1002/pro.3290

703 55. Suchard MA, Lemey P, Baele G, Ayres DL, Drummond AJ, Rambaut A. Bayesian phylogenetic and
704 phylodynamic data integration using BEAST 1.10. Virus Evol. 2018;4. doi:10.1093/ve/vey016

705 56. Revell LJ. phytools: an R package for phylogenetic comparative biology (and other things).
706 Methods Ecol Evol. 2012;3: 217–223. doi:10.1111/j.2041-210X.2011.00169.x

707 57. Crooks GE, Hon G, Chandonia J-M, Brenner SE. WebLogo: A Sequence Logo Generator: Figure 1.
708 Genome Res. 2004;14: 1188–1190. doi:10.1101/gr.849004

709

711 **Tables**

712

713 **Table 1**: Virus name and accession numbers of the 20 sobeliviral species and candidate

714 species or genus (*).

715

Family	Genus (N)	Species	Name	NCBI /uniprot nuc accession number	Uniprot accession nb
Solemoviridae	Sobemovirus (21)	Rice yellow mottle virus	RYMV	AJ608207	Q709L0
		Turnip rosette virus	TRoV	NC004553/AY177608	Q80QX5
		Artemisia virus A	ArtVA	NC017914/JN620802	I1WZY5
		Cymbidium chlorotic mosaic virus	CyCMV	LC381945	A0A2Z6E9A6
		Papaya lethal yellowing virus	PLYV	NC018449/JX123318	J7GBL4
		Xufa yellow dwarf virus	XYDV	ON828429	A0A977KCX8
	Polerovirus (26)	Potato leafroll virus	PLRV	AF453394/X74789	Q84837
		Beet chlorosis virus	BChV	NC002766/MH271171	A0A385L367
		Beet mild yellowing virus	BYMV	NC003491/DQ132996	Q45GB9
		Cereal yellow dwarf virus RPS	CYDV	NC002198/AF235168	Q9IZF5
	Enamovirus (5)	Pea enation mosaic virus 1	PeMV	MN497823	A0A6M8PM86
		Alfalfa enamovirus 1	AlEV	/KU297983	A0A166J1Q2
		Citrus vein enation virus	CVEV	/HF679486	S0EQ55
		Grapevine enamovirus 1	GREnV	/KX645875	A0A1B3B596
	Polemovirus (1)	Poinsettia latent virus	PnLV	AJ867490	Q5NDM9
	Hubsclerovirus (1)	Hubei sclerotinia RNA virus 1	HUSRV	/MK889164	A0A649X039
		Erysiphe necator associated sobemo-like virus 4*	EnAV*	/MN630192	A0A8E3YYS7
Barnaviridae	Barnavirus (1)	Mushroom bacilliform virus	MBV	NC001633/U07551	Q9YPD4
		Rhizoctonia solani barnavirus 1*	RsBV*	/KP900904	A0A0M4KGX8
		Colobanthus quitensis associated barnavirus 1*	CoBV*	MG686618	A0A2P1JMX2

716

717 **Table 2**: Accession numbers of the 5 additional proteins found as homologues of RdRp
718 sobeliviral by AlphaFold

Candidate species	Abbreviation	Uniprot access nb	Source	Reference
Mycroft virus	MyCV	A0A5B8XAH7	arthropods	Harvey et al. 2019
Beihai shrimp virus 5	BeSV	A0A1L3KE75	invertebrates	Shi et al. 2016
Xingshan nematode virus 5	XINV	A0A1L3KF94	invertebrates	Shi et al. 2016

719

720 **Table 3** : Clade-specific residues. Strictly conserved residues and shared sites were indicated
721 (bold and underligned, respectively). Position numbers referred at the structural alignment of
722 the 99 sobelivirales sequences (without the 3 outgroups, see S11 File).

	Sobarnaviruses	Polenamoviruses
Palm		
motifs (A, B, C, D)	I<u>354</u>,S<u>468</u>,K489	**C<u>354</u>**, A<u>468</u>
other sites	**P99,E365**,H486	**A286,F323,D368,N374,T377,R390,W393,**L478
Fingers		
motifs (F,G,H)	S<u>188</u>,**P189**	**G<u>188</u>,K263**
other sites	V<u>205</u>	W25,G26,W<u>205</u>,N529,S561

723

724 **Figure captions**

725 **Figure 1:** RdRp 3D models colored by per-residue model confidence score (local distance
726 difference test, plDDT). The regions modeled with high confidence (plDDT>90) are shown
727 dark blue. The regions colored light blue (plDDT>80) and green (plDDT>70) were modeled
728 with confidence whereas yellow (plDDT>60) and orange (plDDT>50), confidence was low.
729 RYMV (Sobemovirus), PLRV (Polerovirus), PeMV (Enamovirus), MBV (Barnavirus),
730 HuSRV (Hubsclerovirus), XyNV (outgroups).

731 **Figure 2:** Comparison of RdRp 3D model and structures. RdRp domains, palm, fingers and
732 thumb, are colored on RYMV model, grey, purple and pink, respectively. The RdRp
733 picornavirales feature was conserved i.e., index finger structure interacted with the top of the
734 thumb and trapped the ring finger underneath it (black arrows). RdRp structures of
735 picornaviruses (PDB 1RA6, Poliovirus and PDB 1U09, Foot-and-mouth disease virus) are
736 compared to RYMV model and colored based on root mean square deviations (RMSD). The
737 regions with high local structural similarity (RMSD<1Å) are shown dark blue. The regions
738 colored light blue (1<RMSD<2) and green (2<RMSD<3) were similar whereas colored other
739 colors, similarity was low. The α-helix of picornaviruses located at the carboxy-terminal
740 extremity (thumb domain) was lacking in RdRp sobelivirales (shown red). The orientation of
741 the pinky finger in the RYMV predicted structure was closer to FMDV rather than PV (grey
742 arrows).

743 **Figure 3:** Superimposition of RdRp 3D models by genera (a) Sobemovirus (6 ICTV recognized
744 or candidate species), (b) Poler/movirus (5 species), (c) Enamovirus (4 species), (d)
745 Hubsclerovirus (2 recognized or candidate species), (e) Barnavirus (3 recognized or candidate
746 species), (f) outgroups (3 candidate species). Models were colored using standard rainbow code
747 (from N-terminus, dark blue, to C-terminus, red). Major variable segments are pointed out at
748 the intra-genera scale (black arrows) or between outgroups (white arrows).

749 **Figure 4:** Inter-genera superimposition of RdRp 3D models. For clarity reason, only one model
750 per genera was represented (sobemovirus RYMV, poler/movirus PLRV, enamovirus PeMV,
751 barnavirus, hubsclerovirus HuSRV) and only the regions of interest were colored using standard
752 rainbow code (see text). Grey arrows indicated regions with intra-genera variability (as reported
753 in Fig 3), black arrows pointed out regions with inter-genera variability. Highlighted in a circle,
754 the amino-terminal extremity of RdRps forms a conserved β-strand (dark blue) and interacts
755 with other conserved strands of the middle and ring fingers (yellow and green).

756 **Figure 5:** Optimized amino acid alignment of 23 viral RdRps. A-H conserved motifs are
757 framed, strictly conserved residues are indicated in red above. The conservation and RMSD
758 scores were measured at each site and were colored in red and blue to highlight respectively the
759 local similarities and the local differences between both alignments (see Material & Methods).
760 Regions of interest (see text) are figured by arrows, loops or helices.

761 **Figure 6:** Maximum-likelihood phylogenetic tree of sobelivirales based on the structural
762 alignement. The branches are colored according to the five genera and the outgroups. Number
763 at each node indicates bootstrap values based on 100 replicates (only values above 80 are
764 indicated).

765 **Figure 7:** PoW-transformed time tree of the 20 sobelivirales species. The horizontal blue bars
766 show 95% highest posterior density of the node age.

767 **Figure 8:** Clade-specific residues located on 3D RdRp models. Sobarna- and polena-specific
768 residues confirmed on the 99 dataset were figured as sticks on Cα trace of one representative
769 species (RYMV and AlEV). Sobarna- and polena-specific residues which belonged to
770 conserved motifs were colored red & blue, respectively, clade-specific residues of other
771 domains were colored orange & light blue, respectively. Remarkable residues at positions 263,
772 489 or in interaction 365-486 were indicated by arrows or circled in dotted line (see text).

773 **Figure 9:** Figure 9: Optimized motifs of sobeliviral RdRps. (a) For each conserved motif, RdRp
774 conserved residues were colored (black), additional sobeli-specific residues (purple), sobarna-
775 specific residues (red) and polena-specific residues (blue). Common clade-specific positions
776 were highlighted (yellow open boxes). Each sequence logo consists of stacks of symbols, one
777 stack for each position in the sequence. The overall height of the stack indicates the sequence
778 conservation at that position, while the height of symbols within the stack indicates the relative
779 frequency of each amino at that position. Position numbering referred to the alignment with 20
780 sequences. (b) Conserved motifs were indicated on 3D RdRp models of one representative
781 species of each sobeli-clade (sobarna-, RYMV and polena-, AlEV, respectively). Color code
782 was conserved, except clade-specific polymorphic positions colored yellow (arrows).
783 Additional sobeli-specific residues (purple) are circles in dotted lines.

784 **Supporting information**

785 **S1 Table :** Taxonomy and biological characteristics in the phylum Pisuviricota.

786 **S2 Figure :** Back side of RdRp 3D models colored by per-residue model confidence score.
787 Color code is similar to Figure 1. RYMV (Sobemovirus), PLRV (Polerovirus), PeMV
788 (Enamovirus), MBV (Barnavirus), HuSRV (Hubsclerovirus), XyNV (outgroups).

789 **S3 File :** Local pLDDT scores of representative Alphafold models
790 https://pat.cbs.cnrs.fr/sobemo/plddt.html

791 **S4 Figure :** Local Distance Difference Test (pLDDT) data for 5 models of the HcRNAV and
792 RYMV RdRps arranged according to rank by the AlphaFold algorithm.

793 **S5 Figure :** Back side of RYMV RdRp 3D model and picornaviral structures. PDB 1RA6,
794 Poliovirus and PDB 1U09, Foot-and-mouth disease virus. Color code is similar to Figure 2.

795

796 **S6 File :** RMSD between RYMV Alphafold model and PDB templates

797 https://pat.cbs.cnrs.fr/sobemo/rmsd.html

798 **S7 File :** Sequence, secondary structure and solvent accessibility alignments built using

799 mTM-align and STRIDE

800 https://pat.cbs.cnrs.fr/sobemo/align_2d.html

801 **S8 File :** Nucleic acid alignment derived from the amino acid alignment of the 23 Alphafold

802 models

803 https://pat.cbs.cnrs.fr/sobemo/align_dna.fasta

804 **S9 Figure :** Inter-genera superimposition of RdRp 3D models. For clarity reason, only one

805 model per genera was represented (sobemovirus RYMV, poler/movirus PLRV, enamovirus

806 PeMV, barnavirus, hubsclerovirus HuSRV). Major residues of conserved motifs were

807 indicated as black sticks and displayed alone.

808 **S10 File :** Subgroup-conserved amino acids colored and projected on RYMV 3D model

809 https://pat.cbs.cnrs.fr/sobemo/bipart

810 **S11 Table :** Additionnal 79 sequences (genus, name species and accession numbers).

811 **S12 Table :** Clade-specific residues. Strictly conserved residues and shared sites were

812 indicated (bold and underligned, respectively). Position numbers referred at the structural

813 alignment of the 20 sobelivirales sequences (without the 3 outgroups, see S13 File).

814 **S13 File** : MAFFT alignment of 119 sobeliviral RdRps

815 https://pat.cbs.cnrs.fr/sobemo/homologs.html

816

817 **S14 File :** Comparison of mTM-align structural alignment with MAFFT, Clustal Omega and

818 MUSCLE sequence alignments

819 https://pat.cbs.cnrs.fr/sobemo/align_comp.html

820 **S15 Figure :** Phylogenetic tree of sobelivirales based on the structural, MAAFT, Clustalo and

821 Muscle alignements.

822 **S16 File** : RMSD between six sobeliviral and two tombusviral Alphafold RdRp models

823 (BYDV-pav, Luteovirus, and RCNMV, Dianthovirus)

824 https://pat.cbs.cnrs.fr/sobemo/rmsd_bydv_rcnmv

Figure 1

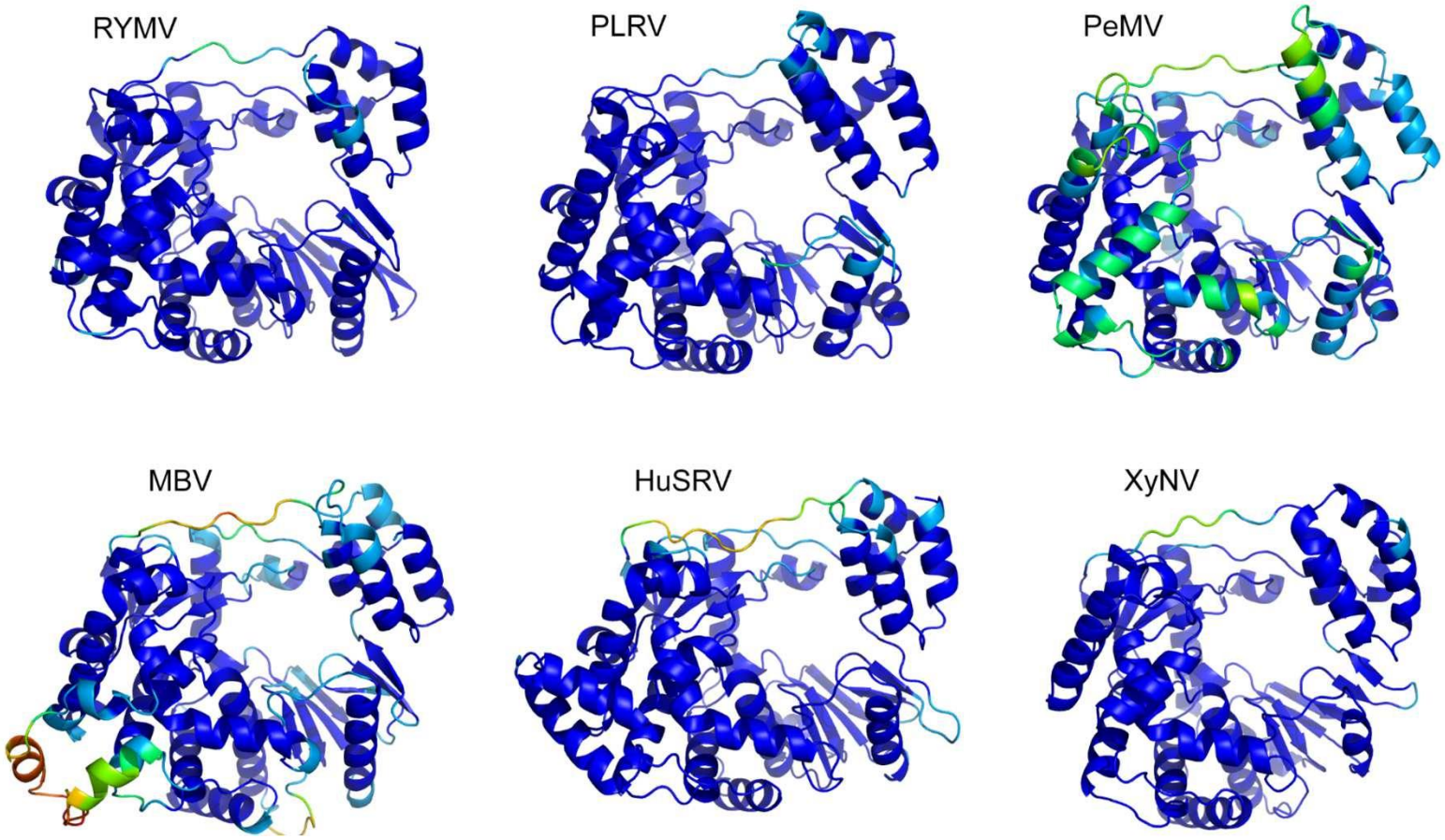

Figure 2

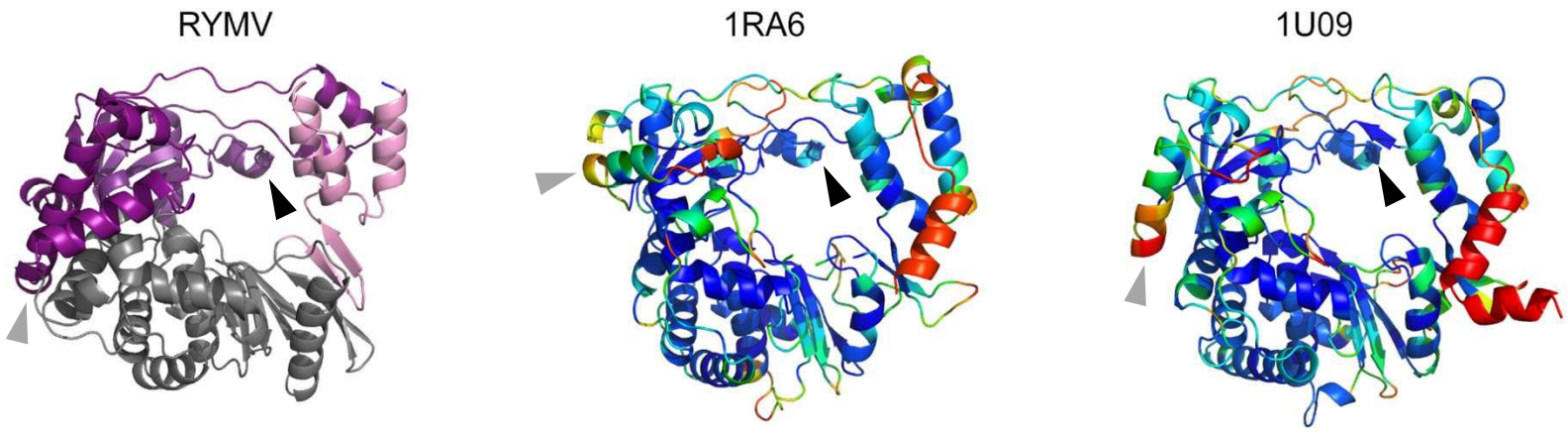

Figure 3

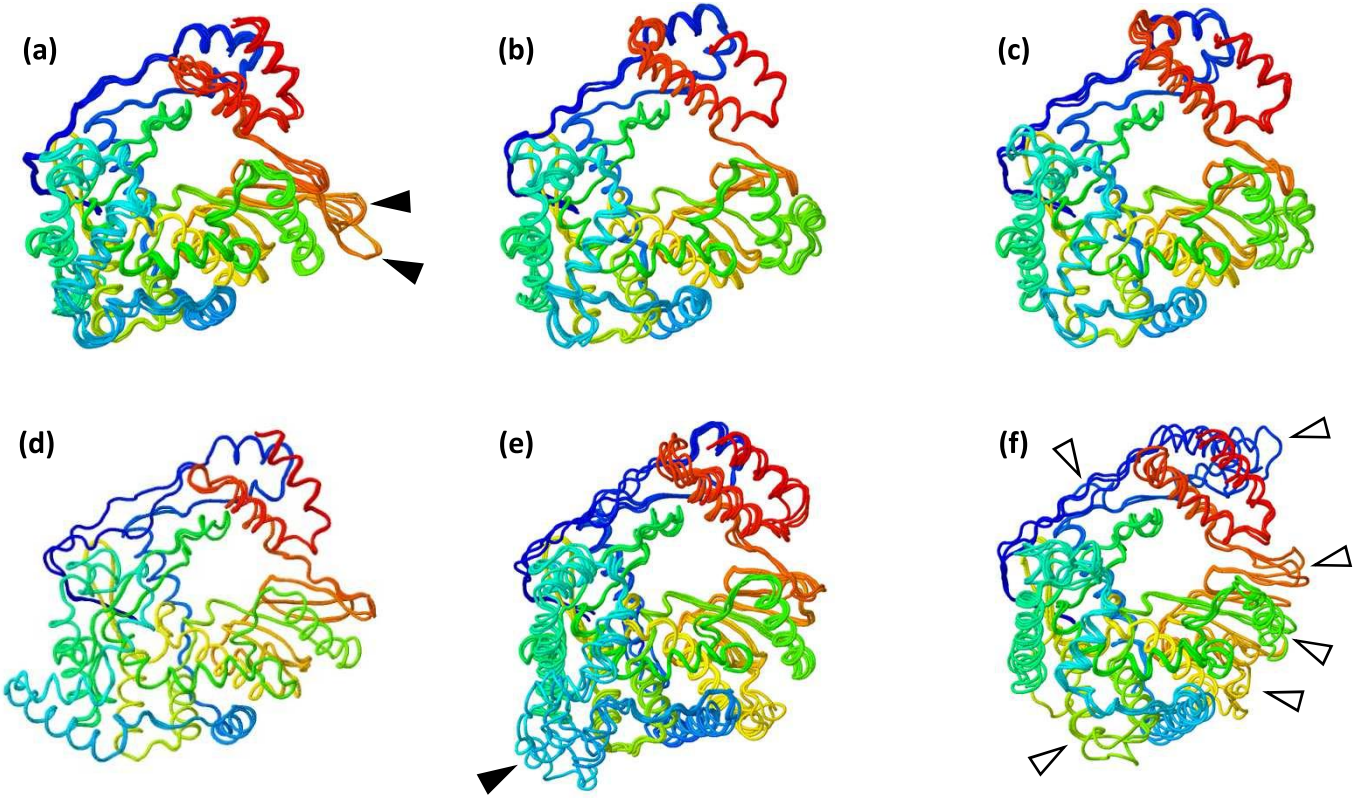

Figure 4

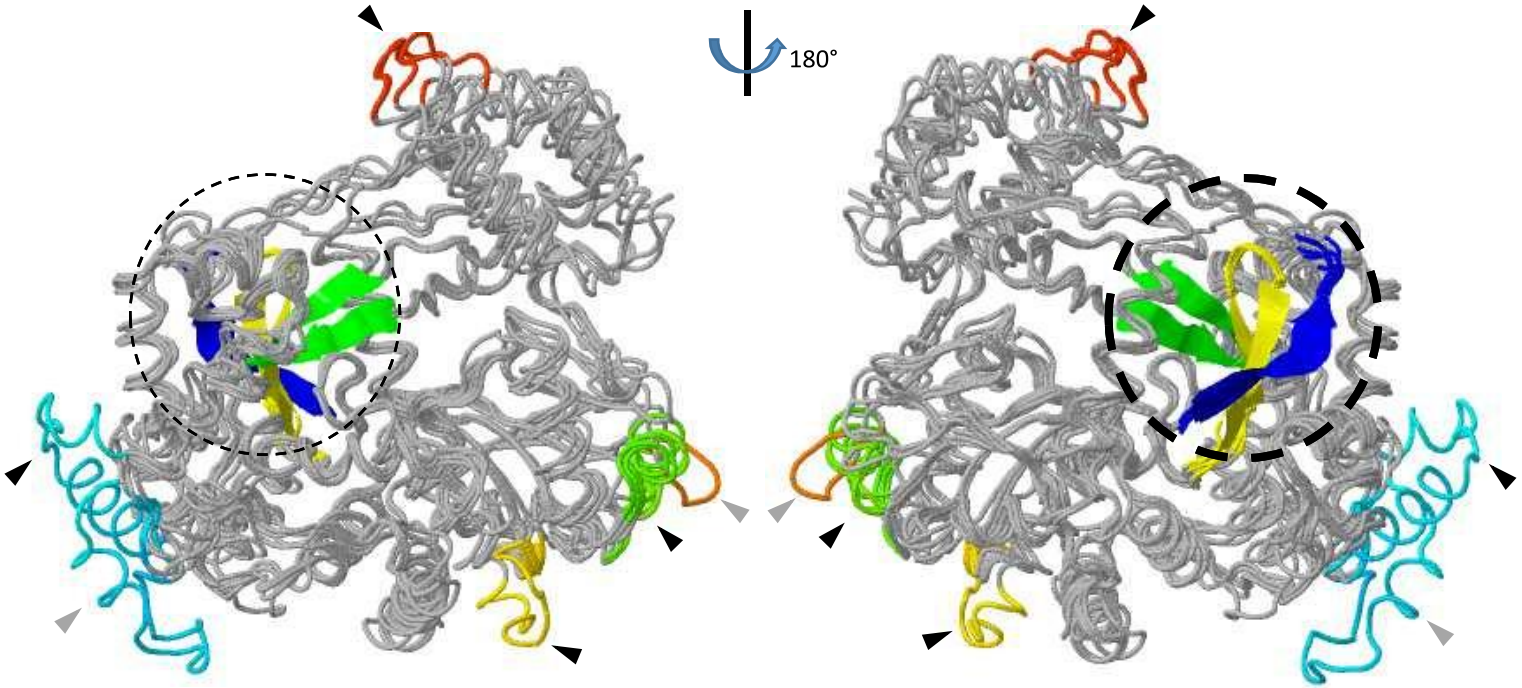

Figure 5 part I

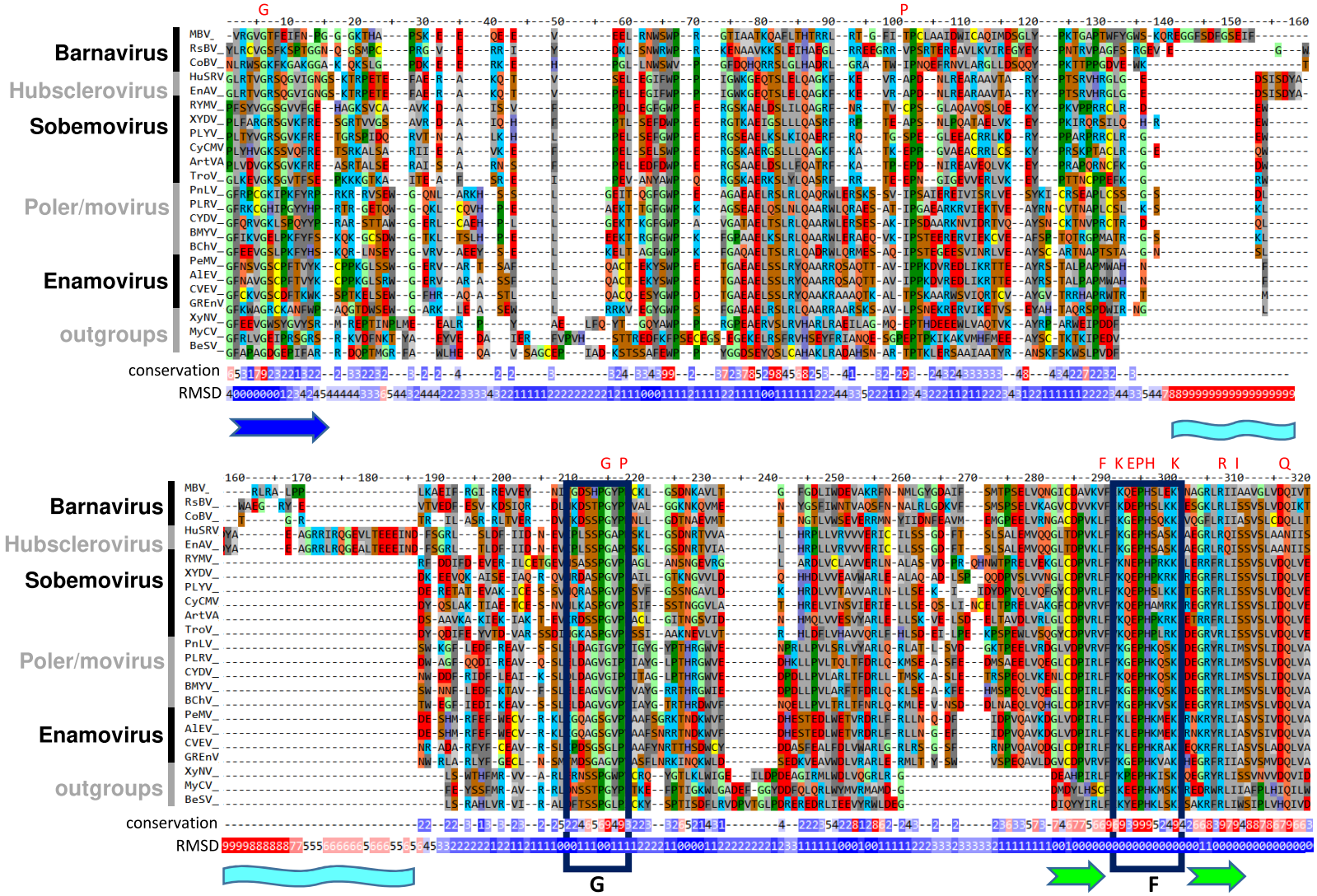

Figure 5 part II

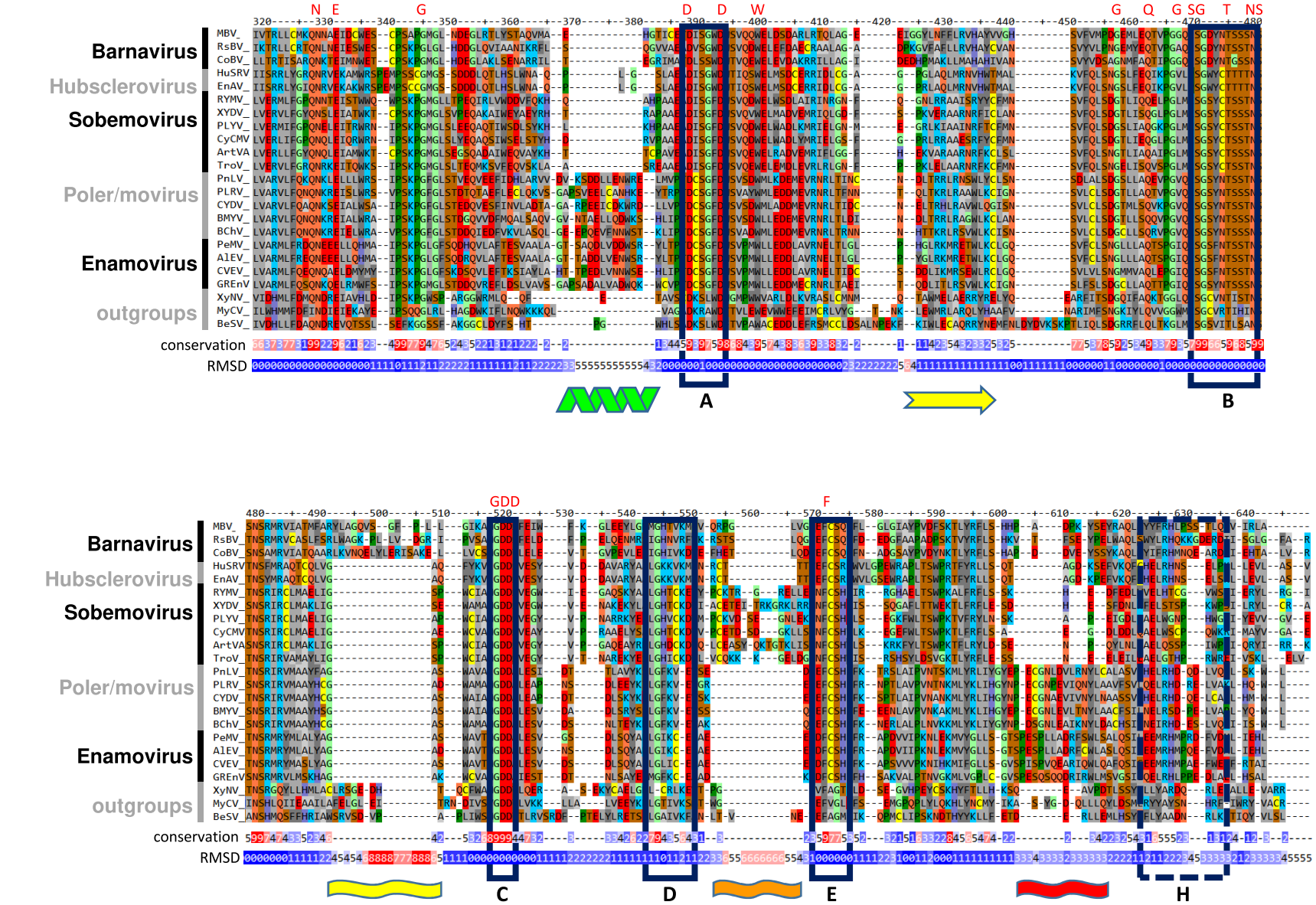

Figure 6

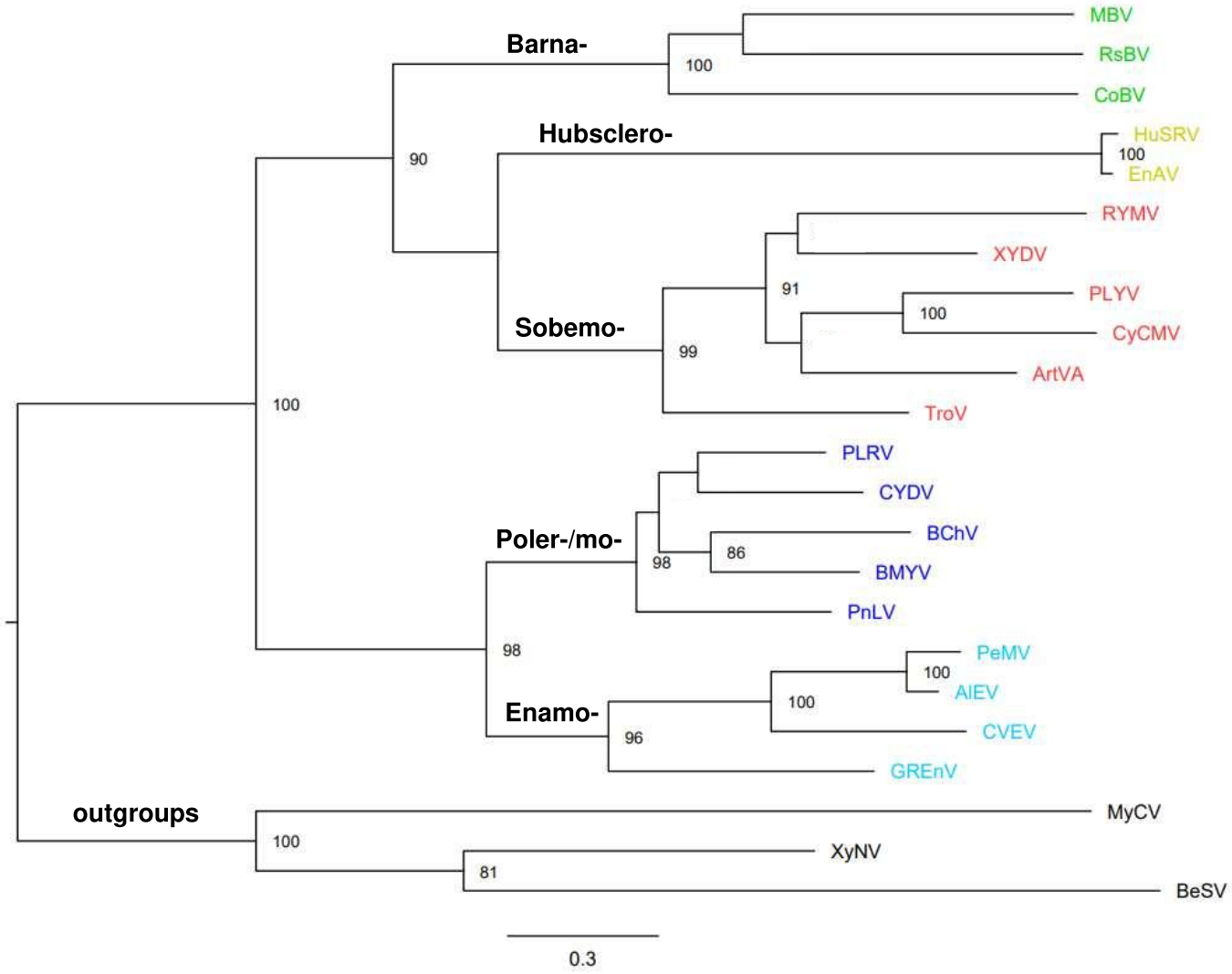
Barna-
MBV
RsBV
CoBV
100
Hubsclero-
HuSRV
EnAV
100
90
RYMV
XYDV
91
PLYV
100
CyCMV
Sobemo-
99
ArtVA
TroV
100
PLRV
CYDV
Poler-/mo-
BChV
86
98
BMYV
PnLV
98
PeMV
100
AlEV
Enamo-
100
CVEV
96
GREnV
outgroups
MyCV
100
XyNV
81
BeSV
0.3

Figure 7

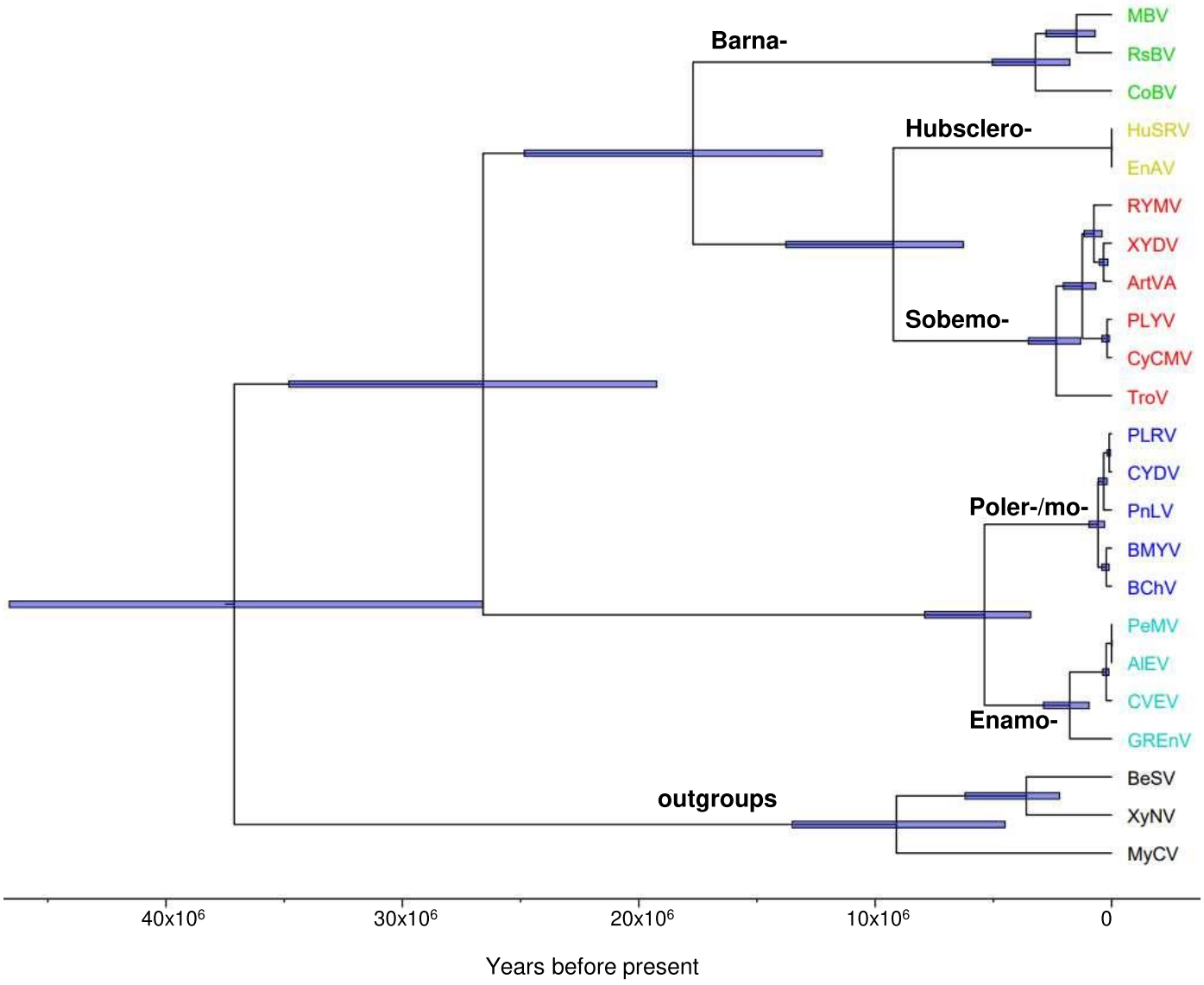
Barna-
Hubsclero-
Sobemo-
Poler-/mo-
Enamo-
outgroups
MBV
RsBV
CoBV
HuSRV
EnAV
RYMV
XYDV
ArtVA
PLYV
CyCMV
TroV
PLRV
CYDV
PnLV
BMYV
BChV
PeMV
AlEV
CVEV
GREnV
BeSV
XyNV
MyCV
40x10⁶
30x10⁶
20x10⁶
10x10⁶
0
Years before present

Figure 8

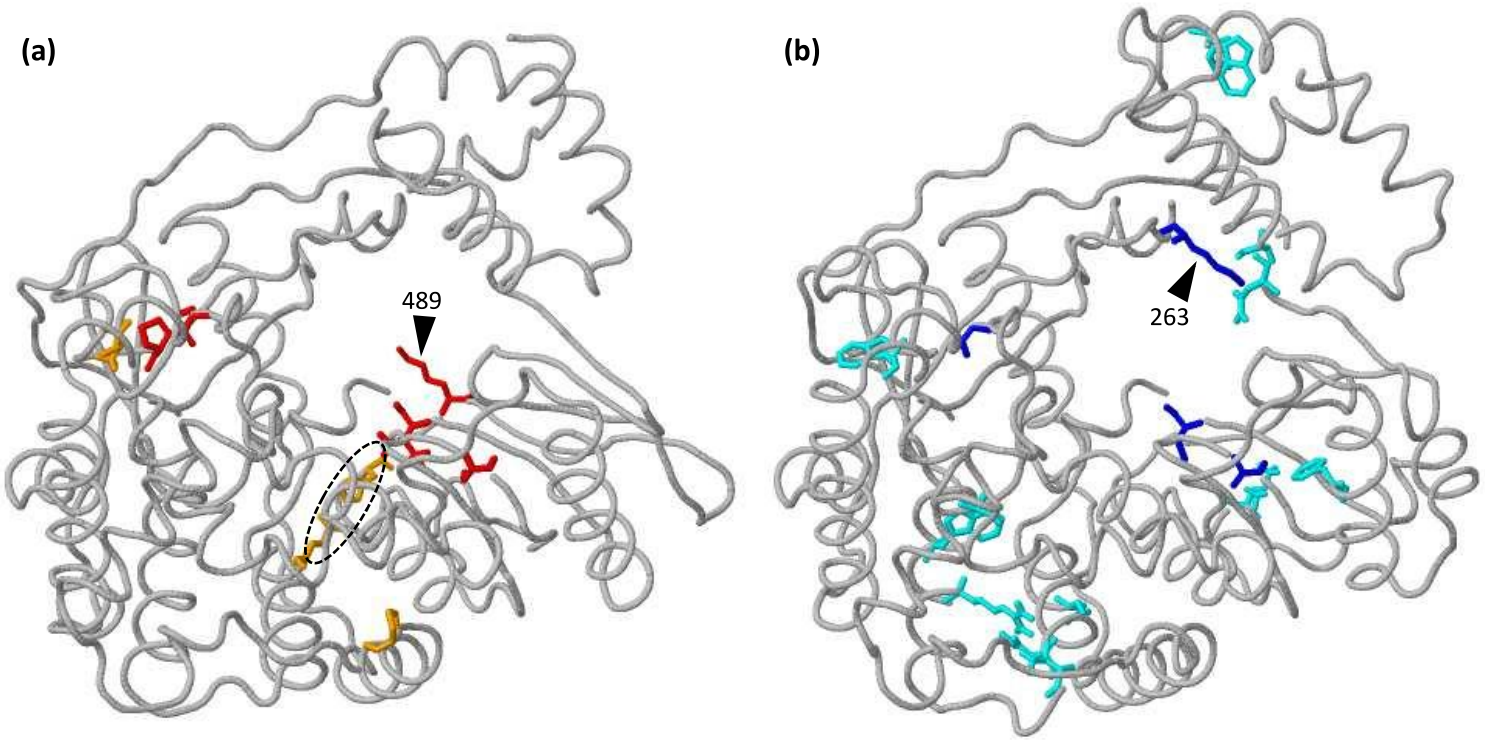

Figure 9

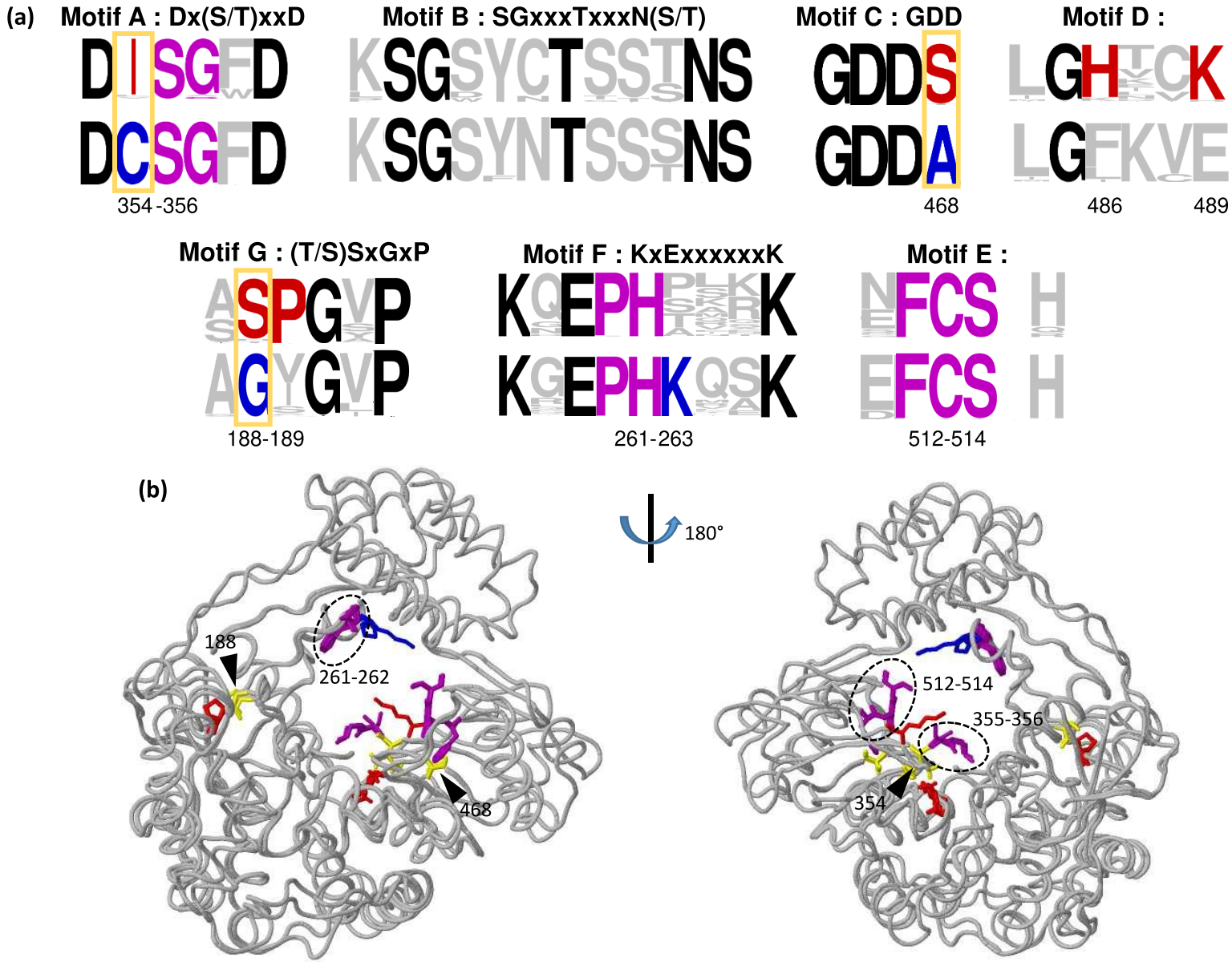
(a)
Motif A : Dx(S/T)xxD
Motif B : SGxxxTxxxN(S/T)
Motif C : GDD
Motif D :
354-356
468
486
489
Motif G : (T/S)SxGxP
Motif F : KxExxxxxxK
Motif E :
188-189
261-263
512-514
(b)
180°
188
261-262
468
512-514
355-356
354